# Steering LVLMs via Sparse Autoencoder for Hallucination Mitigation

# Zhenglin Hua<sup>1</sup>, Jinghan He<sup>2,3</sup>, Zijun Yao<sup>4</sup>, Tianxu Han<sup>5</sup>, Haiyun Guo<sup>2,3</sup>, Yuheng Jia<sup>1</sup>, Junfeng Fang<sup>6</sup>

<sup>1</sup>School of Computer Science and Engineering, Southeast University
 <sup>2</sup>Foundation Model Research Center, Institute of Automation, Chinese Academy of Sciences
 <sup>3</sup>School of Artificial Intelligence, University of Chinese Academy of Sciences
 <sup>4</sup>Department of Computer Science and Technology, Tsinghua University
 <sup>5</sup>Wuhan University of Technology
 <sup>6</sup>National University of Singapore

huazhenglin2003@gmail.com, hejinghan2022@ia.ac.cn

#### **Abstract**

Large vision-language models (LVLMs) have achieved remarkable performance on multimodal tasks such as visual question answering (VQA) and image captioning. However, they still suffer from hallucinations, generating text inconsistent with visual input, posing significant risks in real-world applications. Existing approaches to address this issue focus on incorporating external knowledge bases, alignment training, or decoding strategies, all of which require substantial computational cost and time. Recent works try to explore more efficient alternatives by adjusting LVLMs' internal representations. Although promising, these methods may cause hallucinations to be insufficiently suppressed or lead to excessive interventions that negatively affect normal semantics. In this work, we leverage sparse autoencoders (SAEs) to identify semantic directions closely associated with either hallucinations or actuality, realizing more precise and direct hallucination-related representations. Our analysis demonstrates that interventions along the faithful direction we identified can mitigate hallucinations, while those along the hallucinatory direction can exacerbate them. Building on these insights, we propose Steering LVLMs via SAE Latent Directions (SSL), a training-free method based on SAE-derived latent directions to mitigate hallucinations in LVLMs. Extensive experiments demonstrate that SSL significantly outperforms existing decoding approaches in mitigating hallucinations, while maintaining transferability across different model architectures with negligible additional time overhead.

# 1 Introduction

LVLMs (Liu et al., 2023; Dai et al., 2023b; Liu et al., 2024b) have demonstrated impressive capabilities in jointly processing visual and textual modalities, achieving strong performance on tasks such as VQA (Antol et al., 2015) and image cap-

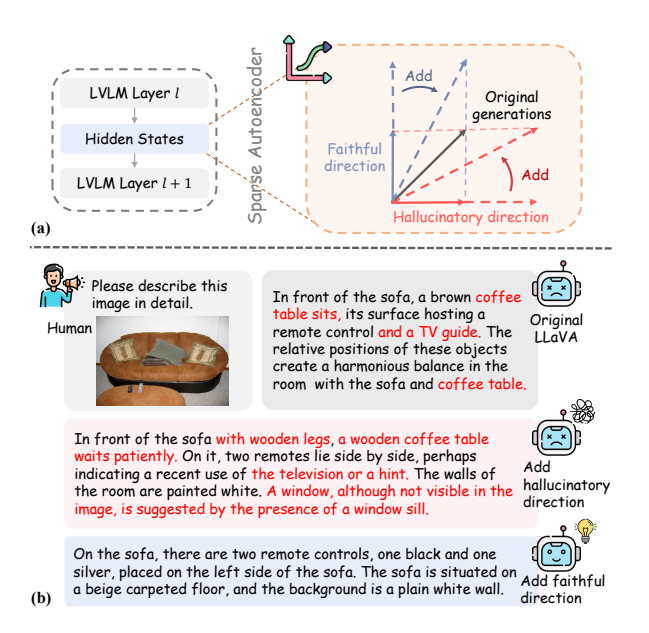


Figure 1: The figure shows, from top to bottom, the original response from the LLaVA-Next-8b, the response after intervention along the hallucinatory direction, and the response after intervention along the faithful direction. These results demonstrate that targeted interventions along faithful directions suppress hallucinatory generations, while perturbations along hallucinatory directions tend to elicit more factually incorrect content.

tioning (Li et al., 2022). However, LVLMs still suffer from hallucination (Yin et al., 2011), where the generated text does not align with the visual content. This limitation poses significant challenges to their deployment in critical applications, including medical diagnosis(Gu et al., 2024) and autonomous driving(You et al., 2024), where factual consistency and reliability are essential.

To mitigate hallucination in LVLMs, researchers explore various strategies, including refining decoding algorithms (Leng et al., 2024; Huang et al., 2024; Kim et al., 2024), incorporating external knowledge bases (Qu et al., 2024), and leveraging additional annotated data for model fine-tuning (Park et al., 2024). While promising, these ap-

proaches often incur substantial computational cost and time. Recent works (Liu et al., 2025; Jiang et al., 2024; Li et al., 2025) try to explore more efficient alternatives by adjusting LVLMs' internal representations. However, these methods may cause hallucinations to be insufficiently suppressed or lead to excessive interventions that negatively affect normal semantics. Therefore, extracting finegrained and reliable representations related to hallucinations remains a key challenge in advancing the reliability of LVLMs.

We note the success of SAEs in extracting fine-grained semantic representations—specifically capturing whether the model knows certain entities—of abstract concepts in the field of large language models (LLMs) (Ferrando et al., 2025). Inspired by this work, we extend the application of SAE-based analysis from LLMs to LVLMs, aiming to understand and mitigate hallucinations more precisely and directly by identifying and steering the internal semantic directions associated with hallucinatory and faithful content. Notably, SAEs builds on the Linear Representation Hypothesis (Park et al., 2023), which posits that internal model representations can be expressed as sparse combinations of interpretable semantic directions (Tigges et al., 2024; Li et al., 2023a). Specifically, we leverage the SAE provided by Zhang et al. (2024a) to identify latent directions that closely correlate with hallucinatory semantics as well as those aligned with faithful content. As illustrated in Figure 1, targeted interventions along faithful directions suppress hallucinatory generations, while perturbations along hallucinatory directions tend to elicit more factually incorrect content.

Building on this insight, we propose Steering LVLMs via SAE Latent Directions (SSL), a training-free approach based on SAE-derived latent directions to mitigate hallucinations in LVLMs. During the visual feature merging stage, we inject faithful semantic directions to amplify grounded semantic features and improve image-text consistency. In the subsequent language generation stage, we reduce projection onto hallucinatory semantic directions, thereby reducing the risk of generating factually incorrect content. Remarkably, although the SAE was trained on the LLaVA-Next-8b model, the extracted hallucination and factuality directions generalize seamlessly to other architectures (e.g., LLaVA1.5-7b model (Liu et al., 2024c) and InstructBLIP-7b model (Dai et al., 2023a)). Experimental evaluation on established LVLM hallucination benchmarks shows that SSL outperforms existing decoding approaches, confirming its effectiveness and efficiency in hallucination reduction.

Our main contributions are as follows:

- We leverage SAEs to identify semantic directions that are highly correlated with hallucinatory and faithful object words in the representation space of LVLMs.
- We propose SSL, a training-free method that injects factuality semantic directions during visual feature fusion to reinforce grounded content and suppresses hallucination directions during language generation to proactively mitigate hallucinatory outputs.
- Extensive experiments demonstrate that SSL outperforms existing decoding approaches on widely used hallucination benchmarks with negligible time overhead, exhibiting transferability across different architectures.

# 2 Preliminary

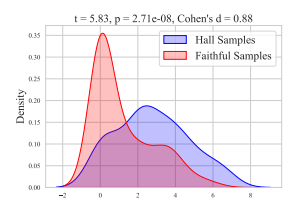
**LVLM generation.** LVLMs take both image and text as input and encode them into a sequence of tokens. During autoregressive generation, the model first concatenates the system tokens  $X_s$ , prompt tokens  $X_t$ , and visual tokens  $X_v$  in a predefined order to form the initial input. At the first generating step t=1, the model predicts the output token based on this initial context. At each subsequent step t>1, the previously generated tokens  $X_o^{< t}$  are appended to the end of the initial input, resulting in the current sequence  $\left[X_s, X_t, X_v, X_o^{< t}\right]$ . The model then generates the next token autoregressively according to the conditional probability distribution, continuing until an end-of-sequence token is produced or a maximum sequence length is reached:

$$y_t = \arg\max p_{\theta}(y_t \mid X_s, X_t, X_v, X_o^{< t}), \quad (1)$$

where  $y_t$  is the token generated at time step t.

**Sparse autoencoders.** SAEs have been proven to be effective for separating overlapping features (Bricken et al., 2023; Ferrando et al., 2025). In this work, we use the SAE provided by Zhang et al. (2024a), which operates on the residual stream  $h_l \in \mathbb{R}^d$  from the l-th layer of LVLMs. The SAE projects these representations into a higher-dimensional latent space  $z(x) \in \mathbb{R}^{d_{\text{SAE}}}$  and applies a ReLU activation:

$$z(x) = \text{ReLU}(W_{\text{enc}}x + b_{\text{enc}}), \tag{2}$$





(a) Hallucinatory latent KDE distribution

(b) Faithful latent KDE distribution

Figure 2: KDE plots of the selected latent activations for test samples labeled as hallucination and faithfulness. The overlaid plots visualize the distributional differences, with annotated t-statistic, p-value, and Cohen's d effect size indicating the statistical separation between the two groups.

where  $W_{\rm enc}$  and  $b_{\rm enc}$  denote the encoder's weight matrix and bias, respectively. To enforce sparsity, a top-k operation retains only the k largest activations in z(x), zeroing out the rest to obtain the sparse latent vector  $z_k(x) = {\rm TopK}(z,k)$ . The decoder then reconstructs the original representation via a linear combination of the active components:

$$SAE(x) = W_{dec}^T z_k(x) + b_{dec}, \qquad (3)$$

where  $W_{\rm dec}$  and  $b_{\rm dec}$  denote the decoder's weight matrix and bias. During training, the loss function combines the reconstruction error with an auxiliary loss proposed by Gao et al. (2025), aiming to encourage the utilization of meaningful features in the latent representation  $z_k(x)$  and to prevent feature inactivity, thereby enhancing the overall expressiveness of the sparse encoding. We refer to each component of  $z_k(x)$  as a latent activation, and each row vector of  $W_{\rm dec}$  as a latent direction.

Steering with SAE Latents. The SAE reconstructs model representations as a linear combination of latent directions and a bias, effectively approximating the original input. Each latent activation  $z_j(x)$  corresponds to a specific decoder direction  $d_j = W_{\rm dec}\left[j,:\right]$ , enabling targeted adjustment of the representation through activation steering (Turner et al., 2023). This technique allows us to steer the residual stream by modifying the representation as follows:

$$x_{\text{steer}} \leftarrow x + \alpha d_j,$$
 (4)

where  $\alpha$  is a tunable parameter that determines the strength of the intervention.

#### 3 Method

In this work, we introduce SSL, a training-free method for steering LVLMs. Our method consists of two principal components: semantic directions identification and steering LVLMs via SAE latents.

#### 3.1 Semantic Directions Identification

Residual Stream Dataset Construction for Hallucinations and Faithfulness. To investigate whether there exist directions in LVLMs that are highly correlated with hallucinatory and faithful semantics, we randomly sampled 4,000 imagetext pairs from the MSCOCO dataset (Lin et al., 2014). Using the LLaVA-Next-8b model (Liu et al., 2024d) for the image captioning task, we extract the residual stream representations from the 25<sup>th</sup> layer when the model generated object tokens classified as either hallucinatory or faithful.

Given that a small proportion of object words are tokenized into multiple subword units, we exclude these cases to simplify the analysis. Furthermore, because each sample exhibited an imbalance between the counts of hallucinatory and faithful object terms, we enforce class balance by sampling an equal number of residual vectors from each category per image—text pair. See Appendix A for a description of the process. Finally, we construct a balanced dataset containing 1, 784 samples and divide it into a training set and a test set in a 9:1 ratio, for direction mining and direction effectiveness validation, respectively.

Semantically Hallucinatory and Faithful Direction Identification via SAE. Inspired by Meng et al. (2022); Ferrando et al. (2025), we leverage SAE to identify latent directions aligned with hallucinatory and faithful semantics. Specifically, each residual stream sample from the training set is passed through the SAE, and we record the activation frequency of each latent activation across hallucinatory samples  $\mathcal{X}_{\text{hall}}$  and faithful samples  $\mathcal{X}_{\text{faithful}}$ . For a given latent activation j, its activation frequencies on hallucinatory samples  $f_j^{\text{hall}}$  and faithful samples  $f_j^{\text{faithful}}$  are computed as:

$$f_{j}^{\text{hall}} = \frac{1}{N_{\text{hall}}} \sum_{x \in \mathcal{X}_{\text{hall}}} \mathbb{I}\left(z_{j}(x) > 0\right),$$

$$f_{j}^{\text{faithful}} = \frac{1}{N_{\text{faithful}}} \sum_{x \in \mathcal{X}_{\text{faithful}}} \mathbb{I}\left(z_{j}(x) > 0\right),$$
(5)

where  $N_{\rm hall}$  and  $N_{\rm faithful}$  represent the number of hallucinatory and faithful samples, respectively. To

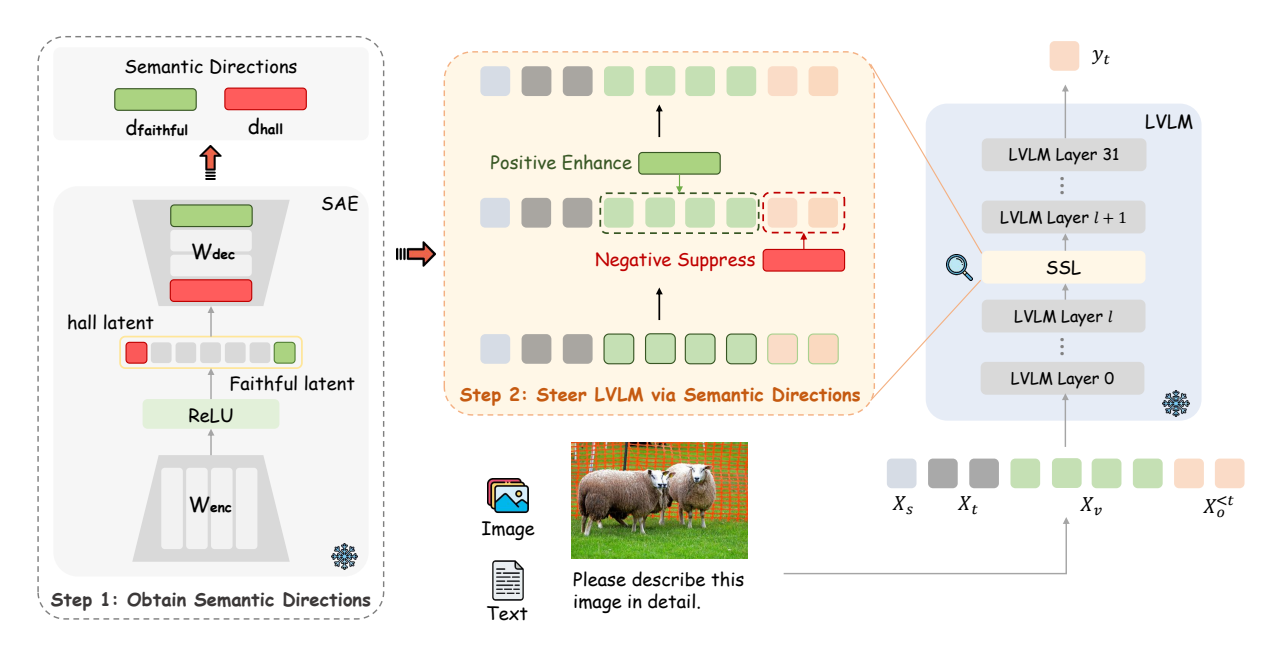


Figure 3: Overview of the proposed SSL approach leveraging SAE to identify semantically aligned directions and mitigate hallucination in LVLMs. We use SAE to identify latent directions within the internal representation space of LVLMs that are associated with hallucinatory and faithful semantics, denoted as  $d_{\text{hall}}$  and  $d_{\text{faithful}}$ , respectively. These semantic directions are then used to modulate the residual stream at the l-th layer, steering the generation process toward greater factual consistency.

quantify the semantic relevance of each latent activation, we compute the difference in activation frequencies as follows:

$$\begin{split} s_{j}^{\text{hall}} &= f_{j}^{\text{hall}} - f_{j}^{\text{faithful}}, \\ s_{j}^{\text{faithful}} &= f_{j}^{\text{faithful}} - f_{j}^{\text{hall}}. \end{split} \tag{6}$$

These values reflect the relevance of latent dimension j to hallucinatory and faithful semantics, respectively. Finally, we identify the latent activation with the highest  $s_j^{\rm hall}$  as the hallucination semantic direction (hereafter referred to as the hall latent), and the one with the highest  $s_j^{\rm faithful}$  as the faithful semantic direction (hereafter referred to as the faithful latent).

Validation of the Effectiveness of Semantic Directions. We begin by analyzing the distributional differences of the hallucinatory latent and faithful latent activations across both sample types in the test set. These distributions are visualized using kernel density estimation (KDE) plots as shown in Figure 2. We further quantify the separation using independent two-sample t-tests and compute Cohen's d to assess effect sizes. Both latent activations exhibit statistically significant distributional shifts, with substantial effect sizes, confirming their discriminative power.

To probe the semantic alignment of the activations, we further conduct Spearman rank correlation analysis between the activation values of hallucinatory samples and their associated hallucinatory object terms. The hallucinatory latent correlates positively with hallucinatory objects (Spearman's  $\rho=0.42,\,p=9.95\times10^{-9}$ ), whereas the faithful latent correlates negatively ( $\rho=-0.44,\,p=9.85\times10^{-10}$ ). Given the binary nature of the labels and the symmetry of rank correlation, we infer a positive correlation between the faithful latent and samples.

Finally, to quantitatively evaluate the predictive power of SAE-derived directions in distinguishing hallucinatory from faithful samples, we design a set of classification experiments based on logistic regression. The model takes the latent activation values—either individually or in combination—as input features for a binary hallucination classification task. As illustrated in Figure 4, the results demonstrate that the latent semantic directions extracted by the SAE are discriminative (see Appendix B for more experimental details). Furthermore, combining the *hall* latent and *faithful* latent as input features yields further performance improvements.

#### 3.2 Steering LVLMs via SAE Latents

**Steering Strategy.** A core architectural mechanism involves multi-layer residual connections that progressively model input information. At each layer, semantic representations are passed through

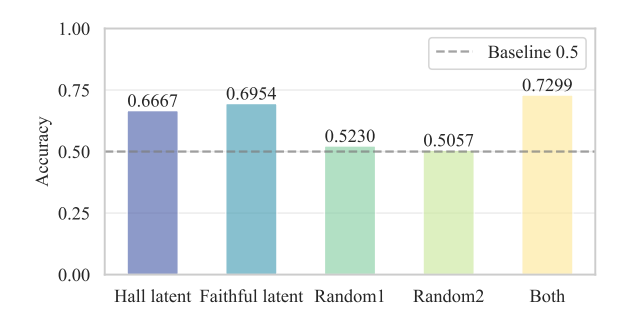


Figure 4: Comparison of classification accuracy using different latent activations. Hall latent and faithful latent correspond to the identified hallucinatory and faithful latent activations, respectively. Random1 denotes a single latent activation randomly selected from the SAE latent space, while Random2 represents a feature combination of two randomly selected latent activations. The dashed line indicates the baseline accuracy of 0.5.

residual flows, which can be divided according to the input sequence into four main components: system token, prompt tokens, visual tokens, and output tokens. Among these, visual tokens interact with language tokens to guide the model's understanding of image content. Injecting faithful direction at this position enables the model to increase visual faithfulness. Output tokens represent the model's autoregressive language generations, influenced by both prompts and visual inputs, thereby reflecting the model's semantic behavior. Suppressing hallucinatory directions during this stage helps reduce hallucination tendencies and enhances factual consistency in language generation.

Following the method described in Section 2, we identify two semantic direction vectors: the hallucinatory direction  $d_{\rm hall}$  and the faithful direction  $d_{\rm faithful}$ . During the visual feature fusion stage, we incorporate  $d_{\rm faithful}$  to improve the faithfulness of visual understanding. In the subsequent language generation stage, we suppress activations along  $d_{\rm hall}$  to reduce the risk of hallucinatory outputs. Semantic steering at layer l is defined as follows:

$$X_{l,v} \leftarrow X_{l,v} + \alpha \cdot d_{\text{faithful}}, X_{l,o}^{< t} \leftarrow X_{l,o}^{< t} - \alpha \cdot d_{\text{hall}},$$
 (7)

where  $\alpha$  is a tunable hyperparameter controlling the strength of semantic steering.

Adaptive Steering Parameters (ASP). The setting of the steering strength  $\alpha$  plays a crucial role in determining the effectiveness of semantic intervention. Traditional steering approaches often rely on a fixed hyperparameter  $\alpha$  to linearly combine the

# **Algorithm 1:** SSL

Input: Scaling factor  $\gamma$ ; steering layer  $l_s$ ; semantic directions  $d_{\text{hall}}, d_{\text{faithful}}$ ; residual stream at layer  $l_s$ :  $[X_{l_s,s}, X_{l_s,t}, X_{l_s,v}, X_{l_s,o}^{< t}]$ 1 if  $L = l_s$  then
2 | for token x in residual stream do
3 | if  $x \in X_{l_s,v}$  then
4 |  $x \leftarrow x + \gamma \cdot \frac{\|x\|}{\|d_{\text{faithful}}\| + \epsilon} \cdot d_{\text{faithful}}$ 

$$\begin{array}{c|c} \mathbf{3} & \qquad \mathbf{if} \ x \in X_{l_s,v} \ \mathbf{then} \\ & \qquad x \leftarrow x + \gamma \cdot \frac{\|x\|}{\|d_{\mathrm{faithful}}\| + \epsilon} \cdot d_{\mathrm{faithful}} \\ \mathbf{5} & \qquad \mathbf{else} \ \mathbf{if} \ x \in X_{l_s,o}^{< t} \ \mathbf{then} \\ & \qquad x \leftarrow x - \gamma \cdot \frac{\|x\|}{\|d_{\mathrm{hall}}\| + \epsilon} \cdot d_{\mathrm{hall}} \\ \mathbf{7} & \qquad \mathbf{else} \\ & \qquad // \ \mathrm{System} \ \mathrm{and} \ \mathrm{prompt} \\ & \qquad \mathrm{tokens} \ \mathrm{remain} \ \mathrm{unchanged} \\ \end{array}$$

steering vector with the residual representations. However, this fixed strategy can result in unstable or suboptimal performance, as the magnitude of residual vectors can vary across model layers and token positions. In such cases, a change that is too small may fail to induce meaningful guidance, while an excessively large change may cause semantic distortion or instability.

To address this limitation, we propose an adaptive feature steering mechanism, which dynamically adjusts the steering strength based on the norm of the residual vector at each token at a given layer. This approach ensures more stable and context-aware intervention across varying model states. Specifically, the adaptive steering strength  $\alpha$  is computed as:

$$\alpha = \gamma \cdot \frac{\|x_{\text{residual}}\|}{\|d_{\text{steer}}\| + \epsilon},\tag{8}$$

where  $\gamma$  is a scaling factor,  $x_{\rm residual}$  denotes the residual vector,  $d_{\rm steer}$  is the steering direction, and  $\epsilon$  is a small constant to avoid numerical instability. An overview of the proposed SSL method is presented in Figure 3. The complete procedure of SSL is provided in Algorithm 1.

# 4 Experiments

#### 4.1 LVLMs

We conduct experiments on three representative LVLMs: LLaVA-NeXT-8b (Liu et al., 2024d), LLaVA-1.5-7b (Liu et al., 2024c) and InstructBLIP-7b (Dai et al., 2023a). These models share a modular structure comprising an image encoder, a pro-

	LLaVA-NeXT-8b		L	LLaVA-1.5-7b		InstructBLIP-7b			
	$CHAIR_S\downarrow$	$CHAIR_I \downarrow$	Avg.Len	$CHAIR_S \downarrow$	$CHAIR_I \downarrow$	Avg.Len	$\mid$ CHAIR $_S \downarrow$	$CHAIR_I \downarrow$	Avg.Len
Greedy	29.60 <sub>±0.89</sub>	$8.03_{\pm0.41}$	165.61	49.44 <sub>±1.57</sub>	$14.19_{\pm 0.76}$	82.97	45.44 <sub>±2.43</sub>	$13.07_{\pm 0.71}$	92.11
Beam	$\underline{27.20}_{\pm 1.19}$	$7.20 \pm 0.39$	174.17	$53.60_{\pm 2.39}$	$15.47_{\pm0.45}$	87.38	$48.68_{\pm 1.65}$	$13.59_{\pm0.43}$	95.92
DoLa	$29.04_{\pm 1.08}$	$7.86_{\pm0.24}$	166.14	$50.64_{\pm 2.33}$	$14.51_{\pm 0.88}$	82.32	46.12±1.85	$13.09_{\pm 0.90}$	91.80
VCD	$31.36_{\pm 1.99}$	$8.40_{\pm 0.79}$	165.43	$51.68_{\pm 1.85}$	$15.29_{\pm0.83}$	83.03	$50.84_{\pm 2.41}$	$14.51_{\pm 0.97}$	91.44
OPERA	-	-	-	$44.04_{\pm 0.94}$	$13.23_{\pm 0.46}$	75.79	$45.88_{\pm 2.31}$	$13.15_{\pm0.87}$	93.51
CODE	$30.76_{\pm0.92}$	$8.09_{\pm0.42}$	158.07	$\overline{47.72}_{\pm 0.79}$	$\overline{14.13}_{\pm 0.56}$	78.43	$50.88_{\pm 2.05}$	$14.21_{\pm 0.92}$	89.62
SSL	<b>25.20</b> ±1.49	<b>6.46</b> ±0.67	162.93	41.08 <sub>±2.11</sub>	12.02 <sub>±0.85</sub>	82.30	38.52 <sub>±4.24</sub>	11.45 <sub>±0.96</sub>	102.62

Table 1: CHAIR results on MSCOCO dataset averaged over 5 random seeds. The best and second-best results are indicated in **bold** and <u>underlined</u>, respectively. *Avg.Len* represents the average length of the generated descriptions.

jection module, and a language model. LLaVA-1.5 and LLaVA-NeXT use an MLP to project all image tokens into the LLM's input space, while Instruct-BLIP employs a Q-Former to select a compact set of informative visual tokens, reducing redundancy. Compared to LLaVA-1.5, LLaVA-NeXT upgrades the LLM from 7b to 8b parameters and supports higher-resolution inputs for visual understanding.

#### 4.2 Benchmarks

**CHAIR.** We evaluate object hallucination using the Caption Hallucination Assessment with Image Relevance (CHAIR) metric (Rohrbach et al., 2018), which compares generated image captions against ground-truth annotations to detect hallucinatory objects mentioned in the captions but absent from the image. CHAIR includes two metrics at both captions level (CHAIR $_I$ ):

$$\begin{aligned} \text{CHAIR}_S &= \frac{|\{\text{captions w/ hallucinatory objects}\}|}{|\{\text{total captions}\}|}, \\ \text{CHAIR}_I &= \frac{|\{\text{hallucinatory objects}\}|}{|\{\text{total mentioned objects}\}|}. \end{aligned} \tag{9}$$

We randomly sample 500 images from the COCO 2014 validation set (Lin et al., 2014) and conduct five runs with different random seeds. For all LVLMs, captions are generated using the prompt "Please describe this image in detail." We report the mean and standard deviation for each metric.

**POPE.** We further evaluate object hallucination using the POPE benchmark (Li et al., 2023b), a question-answering dataset designed to assess the factual consistency of generated image descriptions. POPE contains 500 images from the MSCOCO dataset (Lin et al., 2014), each paired with binary questions of the form: "Is there a <object> in the image?" The dataset comprises three subsets—random, popular, and adversarial—which differ in their object sampling strategies. Model

performance is measured using standard classification metrics: Accuracy, Precision, Recall, and F1 score. To provide an overall assessment, we report the average results across all three subsets.

**LLaVA-Bench.** We evaluate LVLM performance using the LLaVA-Bench (In-the-Wild) benchmark (Liu et al., 2024c), a comprehensive set designed to assess models across diverse and challenging visual scenarios. The benchmark includes 24 images from varied real-world contexts, such as indoor scenes, outdoor environments, and internet memes, paired with 60 carefully curated questions spanning openended QA, fine-grained descriptions, and complex reasoning. We prompt the GPT-40 model to evaluate the LVLMs' outputs along two dimensions: factual accuracy and response detail.

#### 4.3 Baselines

We compare the performance of base LVLMs using greedy decoding and beam search decoding. Additionally, we also conduct a comparison between SSL and the popular training-free approaches that require neither external data nor auxiliary models. Specifically, DoLa (Chuang et al., 2024) derives the next-token distribution by contrasting logits from later and earlier layers; VCD (Leng et al., 2024) employs contrastive learning by comparing the output distributions generated from original and perturbed images; OPERA (Huang et al., 2024) enhances generation quality by alleviating excessive reliance on previously generated tokens during beam search; and CODE (Kim et al., 2024) enhances vision-language alignment by using selfgenerated captions as internal references.

#### 4.4 Implementation Details

We set  $\gamma$  to 0.6, 0.8, and 0.2 for LLaVA-NeXT, LLaVA-1.5, and InstructBLIP, respectively, to balance effective mitigation of hallucination with minimizing the invasiveness of state interventions. SSL

	LLaVA-NeXT-8b F1 score ↑	LLaVA-1.5-7b F1 score ↑	InstructBLIP-7b F1 score ↑
Greedy	89.10	84.99	85.37
Beam	89.30	85.31	84.41
DoLa	89.49	85.08	85.22
VCD	88.91	84.42	84.68
OPERA	-	85.46	84.42
CODE	88.93	84.64	84.81
SSL	89.66	85.44	85.16

Table 2: POPE results averaged over popular, adversarial, and random splits. The best and second-best results are indicated in **bold** and underlined, respectively.

is applied at 16<sup>th</sup> layer for LLaVA-NeXT, 31<sup>th</sup> layer for LLaVA-1.5 and 8<sup>th</sup> layer for InstructBLIP. We faithfully replicate all baseline methods, implementing them based on their open-source codebases and configuring them according to the hyperparameters reported in the original papers. All experimental results are obtained under consistent base model, prompt, and generation parameter settings to ensure a fair comparison. For all methods involving beam search, we set the max\_new\_token to 512 and the beam size to 5.

#### 5 Results

CHAIR. Table 1 reports the performance of SSL on the CHAIR benchmark compared to all baseline approaches. Due to excessive memory requirements, OPERA fails to produce results on LLaVA-NeXT-8b. Notably, although the SAE from Zhang et al. (2024a) were trained on LLaVA-NeXT-8b, the identified semantic directions generalize well across different model architectures. SSL consistently outperforms all baselines across all three LVLMs, while only incurring a marginal trade-off in caption length or descriptive richness.

**POPE.** As shown in Table 2, applying SSL to LVLMs with different architectures consistently improves performance on the POPE benchmark. This demonstrates the robustness of SSL in enhancing models across a spectrum of capabilities and further validates the generalizability of the semantic directions captured by our approach.

**LLaVA-Bench.** Table 3 presents the evaluation results on LLaVA-Bench using GPT-40. The results highlight the effectiveness of SSL in enhancing model accuracy across highly diverse and challenging tasks.

# 5.1 Ablation Study

**Effectiveness of ASP.** To validate the necessity of adaptively adjusting the steering strength, we

	Accuracy ↑	Detailedness ↑
LLaVA-NeXT LLaVA-NeXT w/ SSL	6.2891 <b>6.3671</b>	<b>6.0278</b> 5.2667
LLaVA-1.5 LLaVA-1.5 w/ SSL	<b>5.3333</b> 4.7167	<b>4.7000</b> 4.5667
InstructBLIP InstructBLIP w/ SSL	5.5056 <b>5.5722</b>	4.1111 <b>4.2611</b>

Table 3: Evaluation results on the LLaVA-Bench (Inthe-Wild) benchmark based on prompting GPT-4o.

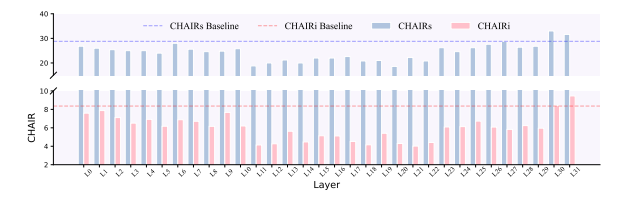


Figure 5: Results of SSL applied across different layers.

conduct an ablation study by replacing ASP with a fixed  $\alpha$  steering parameter as shown in Equation 4 equal to the  $\gamma$  value. As shown in Table 4, removing the adaptive strategy ASP results in consistent performance drops across all three model architectures, highlighting the importance of ASP in effectively mitigating hallucinations.

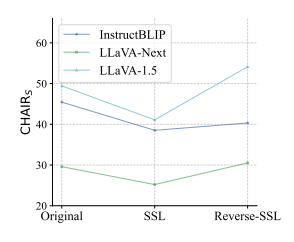
Layer Selection Ablation. We conduct an ablation study on LLaVA-NeXT-8b to examine the impact of applying guidance at different layers. Figure 5 shows that the choice of guidance layer significantly affects model performance, setting  $\gamma$  to 0.8. For LLaVA-NeXT-8b, applying SSL at middle layers yields more effective mitigation of hallucinations, with layer 15 achieving the best performance. For further analysis on steering layer selection and scaling factor  $\gamma$  settings across different models, please refer to Appendix C and D.

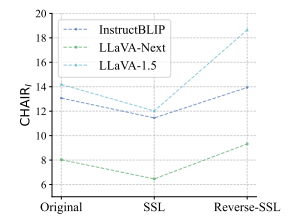
#### 5.2 Further Analysis

Analysis of Reverse-SSL for Inducing Hallucinations in LVLMs. To further validate the effectiveness of the semantic directions we identified, we compare the CHAIR benchmark across three model architectures under three settings: original model state, SSL, and Reverse-SSL (see Appendix E for details on Reverse-SSL). As shown in Figure 6, across all three model architectures, applying Reverse-SSL significantly increases hallucinations, while standard SSL guidance consistently reduces hallucinations. To further clearly illustrate

	$\mid$ CHAIR $_S \downarrow$	$CHAIR_I\downarrow$
LLaVA-NeXT w/ ASP LLaVA-NeXT w/ fixed $\alpha$	<b>25.20</b> 28.40	<b>6.46</b> 7.79
LLaVA-1.5 w/ ASP LLaVA-1.5 w/ fixed $\alpha$	<b>41.08</b> 47.21	<b>12.02</b> 13.12
	<b>38.52</b> 45.40	<b>11.45</b> 12.70

Table 4: Ablation study on the necessity of adaptively adjusting the steering parameters.





- (a) CHAIR<sub>S</sub> across models
- (b) CHAIR<sub>I</sub> across models

Figure 6: CHAIR evaluation across three multi-modal models—InstructBLIP-7b, LLaVA-NeXT-8b, and LLaVA-1.5-7b—under three generation settings: original, SSL, and Reverse-SSL.

the effectiveness of SSL, we present several qualitative examples in Appendix F.

Additional Time Analysis. During each generation step, SSL dynamically adjusts the steering strength through a single scaling and weighting operation, introducing negligible computational overhead. Compared to the overall generation process, the additional latency introduced by SSL is minimal. A comparison of inference time between SSL and other baselines is shown in Figure 7.

# 6 Related Works

LVLMs refer to the phenomenon where the generated textual content is inconsistent with the visual input. This issue arises from various factors, such as dataset bias, insufficient visual perception by the encoder, and misalignment across modalities (Liu et al., 2024a). While prior studies have proposed diverse strategies to mitigate hallucination, the internal mechanisms within LVLMs that give rise to such inconsistencies remain largely underexplored.

Liu et al. (2025) enhance the stability of visual representations by steering latent features during generation, preventing premature degradation. Jiang et al. (2024) remove hallucination-related feature components through linear orthogonalization

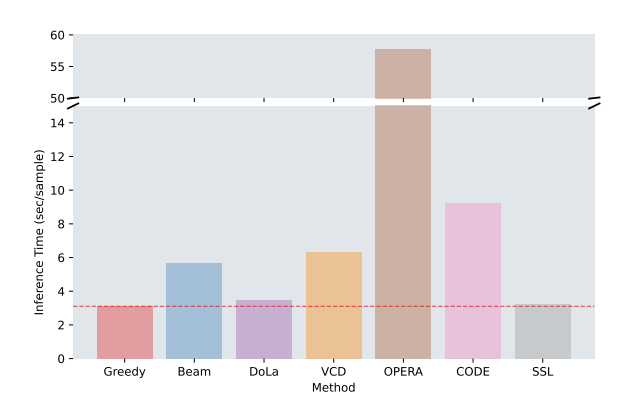


Figure 7: Comparison of inference time for different methods measured using identical hardware.

by projecting the internal image representations of vision models into the language space, thereby purifying the input and reducing hallucinations. Li et al. (2025) uncover phenomena such as early activation and progressive loss of visual information in LVLMs, and propose injecting continuous visual streams during inference to compensate for these effects, significantly reducing hallucinations.

Unlike previous methods, our work directly identifies hallucinatory and faithful semantic directions using SAEs. We then dynamically adjust these directions during visual-linguistic fusion and generation to proactively reduce hallucination outputs.

Furthermore, our approach contributes to the practical interpretability of SAEs in LVLMs, demonstrating their potential for understanding and controlling internal semantic representations.

#### 7 Conclusion

This work explores the relationship between the hallucination in LVLMs and their internal latent representations. We construct a residual stream dataset for hallucinatory and faithful object tokens, and use SAE to extract the semantic directions corresponding to hallucination and Factuality. Based on this insight, we propose SSL, a training-free method that amplifies true semantics while suppressing potential hallucinations. Extensive experiments demonstrate that SSL outperforms existing methods. Furthermore, although the SAE was trained on LLaVA-Next, the semantic directions it extracted generalize well across different model architectures, further showcasing the potential of SAE in understanding and controlling the internal semantic representations of models.

#### Limitations

Currently, the only fully open-source multi-modal SAE is provided by LLM-Labs, trained on the 25<sup>th</sup> layer of the LLaVA-Next 8b model. As a result, our study does not include a comparison of SAEs trained on other model architectures across different multi-modal models. Future work can focus on training multi-modal SAEs on various architectures to investigate whether the findings from this study generalize across different models.

#### **Ethical Consideration**

In our proposed SSL method, positive steering significantly reduces hallucinations in LVLMs, while negative steering increases them. Positive steering not only improves model performance but also aligns with ethical principles such as safety and reliability. In contrast, negative guidance may lead to more hallucinations and generate false information. Therefore, such mechanisms should be applied with caution, supported by thorough validation and human oversight.

#### References

- Stanislaw Antol, Aishwarya Agrawal, Jiasen Lu, Margaret Mitchell, Dhruv Batra, C. Lawrence Zitnick, and Devi Parikh. 2015. VQA: visual question answering. In 2015 IEEE International Conference on Computer Vision, ICCV 2015, Santiago, Chile, December 7-13, 2015, pages 2425–2433. IEEE Computer Society.
- Trenton Bricken, Adly Templeton, Joshua Batson, Brian Chen, Adam Jermyn, Tom Conerly, Nick Turner, Cem Anil, Carson Denison, Amanda Askell, Robert Lasenby, Yifan Wu, Shauna Kravec, Nicholas Schiefer, Tim Maxwell, Nicholas Joseph, Zac Hatfield-Dodds, Alex Tamkin, Karina Nguyen, and 6 others. 2023. Towards monosemanticity: Decomposing language models with dictionary learning. In *Transformer Circuits Thread*.
- Liang Chen, Haozhe Zhao, Tianyu Liu, Shuai Bai, Junyang Lin, Chang Zhou, and Baobao Chang. 2025. An image is worth 1/2 tokens after layer 2: Plug-and-play inference acceleration for large vision-language models. In *Computer Vision ECCV 2024*, pages 19–35, Cham. Springer Nature Switzerland.
- Yung-Sung Chuang, Yujia Xie, Hongyin Luo, Yoon Kim, James R. Glass, and Pengcheng He. 2024. Dola: Decoding by contrasting layers improves factuality in large language models. In *The Twelfth International Conference on Learning Representations*.
- Wenliang Dai, Junnan Li, Dongxu Li, Anthony Tiong, Junqi Zhao, Weisheng Wang, Boyang Li, Pascale

- Fung, and Steven Hoi. 2023a. InstructBLIP: Towards general-purpose vision-language models with instruction tuning. In *Thirty-seventh Conference on Neural Information Processing Systems*.
- Wenliang Dai, Junnan Li, Dongxu Li, Anthony Meng Huat Tiong, Junqi Zhao, Weisheng Wang, Boyang Li, Pascale Fung, and Steven Hoi. 2023b. Instructblip: Towards general-purpose vision-language models with instruction tuning. *ArXiv preprint*, abs/2305.06500.
- Javier Ferrando, Oscar Balcells Obeso, Senthooran Rajamanoharan, and Neel Nanda. 2025. Do i know this entity? knowledge awareness and hallucinations in language models. In *The Thirteenth International Conference on Learning Representations*.
- Leo Gao, Tom Dupre la Tour, Henk Tillman, Gabriel Goh, Rajan Troll, Alec Radford, Ilya Sutskever, Jan Leike, and Jeffrey Wu. 2025. Scaling and evaluating sparse autoencoders. In *The Thirteenth International Conference on Learning Representations*.
- Xuan Gong, Tianshi Ming, Xinpeng Wang, and Zhihua Wei. 2024. Damro: Dive into the attention mechanism of lvlm to reduce object hallucination. *ArXiv preprint*, abs/2410.04514.
- Zishan Gu, Changchang Yin, Fenglin Liu, and Ping Zhang. 2024. Medvh: Towards systematic evaluation of hallucination for large vision language models in the medical context. *ArXiv preprint*, abs/2407.02730.
- Jinghan He, Kuan Zhu, Haiyun Guo, Junfeng Fang, Zhenglin Hua, Yuheng Jia, Ming Tang, Tat-Seng Chua, and Jinqiao Wang. 2024. Cracking the code of hallucination in lvlms with vision-aware head divergence. *ArXiv preprint*, abs/2412.13949.
- Qidong Huang, Xiaoyi Dong, Pan Zhang, Bin Wang, Conghui He, Jiaqi Wang, Dahua Lin, Weiming Zhang, and Nenghai Yu. 2024. OPERA: Alleviating Hallucination in Multi-Modal Large Language Models via Over-Trust Penalty and Retrospection-Allocation. In 2024 IEEE/CVF Conference on Computer Vision and Pattern Recognition (CVPR), pages 13418–13427, Los Alamitos, CA, USA. IEEE Computer Society.
- Nick Jiang, Anish Kachinthaya, Suzie Petryk, and Yossi Gandelsman. 2024. Interpreting and editing vision-language representations to mitigate hallucinations. *ArXiv preprint*, abs/2410.02762.
- Junho Kim, Hyunjun Kim, KIM YEONJU, and Yong Man Ro. 2024. CODE: Contrasting self-generated description to combat hallucination in large multi-modal models. In *The Thirty-eighth Annual Conference on Neural Information Processing Systems*.
- Sicong Leng, Hang Zhang, Guanzheng Chen, Xin Li, Shijian Lu, Chunyan Miao, and Lidong Bing. 2024.

- Mitigating Object Hallucinations in Large Vision-Language Models through Visual Contrastive Decoding . In 2024 IEEE/CVF Conference on Computer Vision and Pattern Recognition (CVPR), pages 13872–13882, Los Alamitos, CA, USA. IEEE Computer Society.
- Junnan Li, Dongxu Li, Caiming Xiong, and Steven Hoi. 2022. Blip: Bootstrapping language-image pretraining for unified vision-language understanding and generation. In *International conference on ma*chine learning, pages 12888–12900. PMLR.
- Kenneth Li, Oam Patel, Fernanda Viégas, Hanspeter Pfister, and Martin Wattenberg. 2023a. Inference-time intervention: Eliciting truthful answers from a language model. In *Thirty-seventh Conference on Neural Information Processing Systems*.
- Yifan Li, Yifan Du, Kun Zhou, Jinpeng Wang, Xin Zhao, and Ji-Rong Wen. 2023b. Evaluating object hallucination in large vision-language models. In *Proceedings of the 2023 Conference on Empirical Methods in Natural Language Processing*, pages 292–305, Singapore. Association for Computational Linguistics.
- Zhuowei Li, Haizhou Shi, Yunhe Gao, Di Liu, Zhenting Wang, Yuxiao Chen, Ting Liu, Long Zhao, Hao Wang, and Dimitris N. Metaxas. 2025. The hidden life of tokens: Reducing hallucination of large vision-language models via visual information steering. *ArXiv preprint*, abs/2502.03628.
- Tsung-Yi Lin, Michael Maire, Serge Belongie, James Hays, Pietro Perona, Deva Ramanan, Piotr Dollár, and C. Lawrence Zitnick. 2014. Microsoft coco: Common objects in context. In *Computer Vision ECCV 2014*, pages 740–755, Cham. Springer International Publishing.
- Hanchao Liu, Wenyuan Xue, Yifei Chen, Dapeng Chen, Xiutian Zhao, Ke Wang, Liping Hou, Rongjun Li, and Wei Peng. 2024a. A survey on hallucination in large vision-language models. *ArXiv preprint*, abs/2402.00253.
- Haotian Liu, Chunyuan Li, Yuheng Li, and Yong Jae Lee. 2024b. Improved baselines with visual instruction tuning. In 2024 IEEE/CVF Conference on Computer Vision and Pattern Recognition (CVPR), pages 26286–26296.
- Haotian Liu, Chunyuan Li, Yuheng Li, and Yong Jae Lee. 2024c. Improved baselines with visual instruction tuning. In *Proceedings of the IEEE/CVF Conference on Computer Vision and Pattern Recognition*, pages 26296–26306.
- Haotian Liu, Chunyuan Li, Yuheng Li, Bo Li, Yuanhan Zhang, Sheng Shen, and Yong Jae Lee. 2024d. Llavanext: Improved reasoning, ocr, and world knowledge.
- Haotian Liu, Chunyuan Li, Qingyang Wu, and Yong Jae Lee. 2023. Visual instruction tuning. *ArXiv preprint*, abs/2304.08485.

- Sheng Liu, Haotian Ye, and James Zou. 2025. Reducing hallucinations in large vision-language models via latent space steering. In *The Thirteenth International Conference on Learning Representations*.
- Kevin Meng, David Bau, Alex J Andonian, and Yonatan Belinkov. 2022. Locating and editing factual associations in GPT. In *Advances in Neural Information Processing Systems*.
- Dongmin Park, Zhaofang Qian, Guangxing Han, and Ser-Nam Lim. 2024. Mitigating dialogue hallucination for large vision language models via adversarial instruction tuning. *ArXiv preprint*, abs/2403.10492.
- Kiho Park, Yo Joong Choe, and Victor Veitch. 2023. The linear representation hypothesis and the geometry of large language models. In *Causal Representation Learning Workshop at NeurIPS* 2023.
- Xiaoye Qu, Qiyuan Chen, Wei Wei, Jishuo Sun, and Jianfeng Dong. 2024. Alleviating hallucination in large vision-language models with active retrieval augmentation. *ArXiv preprint*, abs/2408.00555.
- Anna Rohrbach, Lisa Anne Hendricks, Kaylee Burns, Trevor Darrell, and Kate Saenko. 2018. Object hallucination in image captioning. In *Proceedings of the 2018 Conference on Empirical Methods in Natural Language Processing*, pages 4035–4045, Brussels, Belgium. Association for Computational Linguistics.
- Curt Tigges, Oskar J. Hollinsworth, Atticus Geiger, and Neel Nanda. 2024. Language models linearly represent sentiment. In *Proceedings of the 7th Black*boxNLP Workshop: Analyzing and Interpreting Neural Networks for NLP, pages 58–87, Miami, Florida, US. Association for Computational Linguistics.
- Alexander Matt Turner, Lisa Thiergart, David Udell, Gavin Leech, Ulisse Mini, and Monte MacDiarmid. 2023. Activation addition: Steering language models without optimization. *ArXiv preprint*, abs/2308.10248.
- Shukang Yin, Chaoyou Fu, Sirui Zhao, Ke Li, Xing Sun, Tong Xu, and Enhong Chen. 2011. A survey on multimodal large language models. *ArXiv preprint*, abs/11/12.
- Junwei You, Haotian Shi, Zhuoyu Jiang, Zilin Huang, Rui Gan, Keshu Wu, Xi Cheng, Xiaopeng Li, and Bin Ran. 2024. V2x-vlm: End-to-end v2x cooperative autonomous driving through large vision-language models. *ArXiv preprint*, abs/2408.09251.
- Kaichen Zhang, Yifei Shen, Bo Li, and Ziwei Liu. 2024a. Large multi-modal models can interpret features in large multi-modal models. *ArXiv preprint*, abs/2411.14982.
- Xiaofeng Zhang, Yihao Quan, Chaochen Gu, Chen Shen, Xiaosong Yuan, Shaotian Yan, Hao Cheng, Kaijie Wu, and Jieping Ye. 2024b. Seeing clearly by layer two: Enhancing attention heads to alleviate hallucination in lvlms. *ArXiv preprint*, abs/2411.09968.

# A Construction of Residual Stream Dataset for Hallucinatory and Faithful Object Words

Figure 8 illustrates the construction process of the residual stream dataset. We begin by randomly sampling 4,000 image-text pairs from the MSCOCO dataset and extracting residual stream vectors from the 25th layer of the LLaVA-Next-8b model corresponding to object words identified as either hallucinatory or faithful during inference. It is worth noting that some object words are tokenized into multiple subword tokens by the model's tokenizer. Given the relatively low frequency of such cases and to facilitate consistent statistical analysis, we exclude these incomplete subword instances from our dataset. For example, the word "backpack" may be split into two tokens—"back" and "pack"—by the tokenizer. Since these subtokens do not independently convey the complete semantic meaning of the original word, they are omitted from further analysis.

To ensure class balance, we extract an equal number of residual stream vectors for hallucinatory and faithful object words from each sample. This process results in a balanced dataset comprising 1,784 instances, with a 1:1 ratio of positive (hallucinatory) and negative (faithful) samples. We further divide the dataset into training and test sets using a 9:1 split while maintaining the class distribution in both subsets. The training set is used to identify semantic directions closely associated with hallucination, and the test set is employed to evaluate the generalizability and discriminative power of the extracted semantic features. Using sparse autoencoder analysis, we find that the direction corresponding to latent activation index 36992 is highly correlated with hallucination, whereas index 47230 aligns closely with faithful outputs.

# B A Set of Classification Experiments Based on Logistic Regression

To quantitatively evaluate the discriminative power of the latent activation directions extracted by the SAE in distinguishing hallucinatory from faithful samples, we conduct a series of classification experiments based on logistic regression. Specifically, for the i-th sample, let  $z(x_i) \in \mathbb{R}^{d_{\text{SAE}}}$  denote the SAE latent representation. From a total of N samples, we extract individual latent dimensions indexed by j, denoted as  $z_j(x_i)$ , and construct five types of input features:

Hall latent: The dimension *hall* with the highest correlation to hallucinated object words is selected, forming a one-dimensional feature:

$$X_{\text{hall}} = [z_{\text{hall}}(x_1), \dots, z_{\text{hall}}(x_N)]^T \in \mathbb{R}^{N \times 1}.$$
(10)

Faithful latent: The dimension faithful most correlated with faithful object words is selected, forming:

$$egin{aligned} X_{ ext{faithful}} \ &= \left[ z_{ ext{faithful}}(x_1), \dots, z_{ ext{faithful}}(x_N) 
ight]^T \in \mathbb{R}^{N imes 1}. \end{aligned}$$

Random 1: A single latent dimension  $r_1 \sim \mathcal{U}\{0,\ldots,d_{\text{SAE}}-1\}$  is randomly sampled to form a one-dimensional baseline feature  $X_{r_1} = \mathbb{R}^{N\times 1}$ .

Random 2: Two latent dimensions  $(r_1, r_2)$  are randomly sampled to construct a two-dimensional feature  $X_{r_2} \in \mathbb{R}^{N \times 2}$ .

The corresponding label vector is  $y = [y^{(1)}, y^{(2)}, \dots, y^{(N)}]^T$ , where  $y^{(i)} \in \{0, 1\}$ , with 1 indicating a hallucinatory sample and 0 a faithful sample. All input features are standardized before being fed into the logistic regression model. The model is trained on the training set and evaluated on the held-out test set using classification accuracy and confusion matrices as evaluation metrics.

As shown in Figure 9, the confusion matrices for the three main feature groups (Hall latent, Faithful latent, Both). The results show that the model achieves balanced performance across both positive and negative classes, with no noticeable prediction bias. Figure 4, the performance of Random1 and Random2 approximates the random baseline ( $\approx 0.5$ ), while using Hall latent and faithful latent individually yields classification accuracies of 66.67% and 69.54%, respectively. Combining the two features (Both) further improves performance to 72.99%.

These findings suggest that the latent representations extracted by the SAE encode semantically discriminative signals for hallucination detection. Furthermore, combining hallucination and factuality-related latent directions provides complementary information that enhances classification performance.

#### C Choice of Steering Layer

Figures 10, 11 and 12 present the results of ablation studies investigating the effect of introducing SSL at individual layers of the LLaVA-Next ( $\gamma = 0.6$ ), LLaVA-1.5 ( $\gamma = 0.8$ ) and InstructBLIP

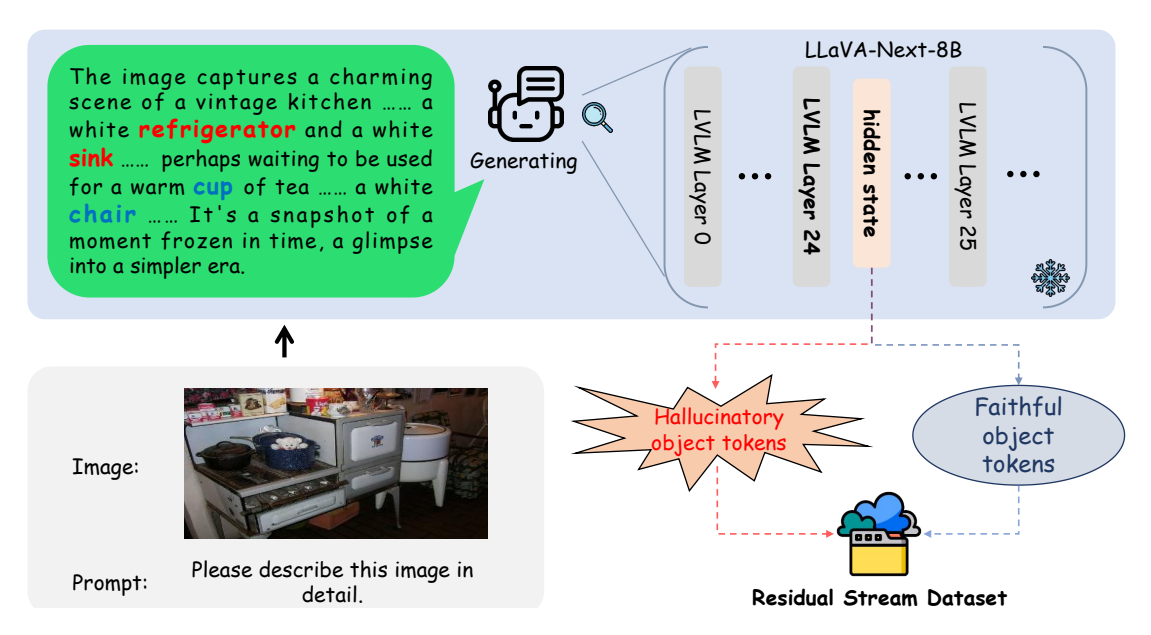


Figure 8: The process of construction of residual stream dataset for hallucinatory and faithful object words.

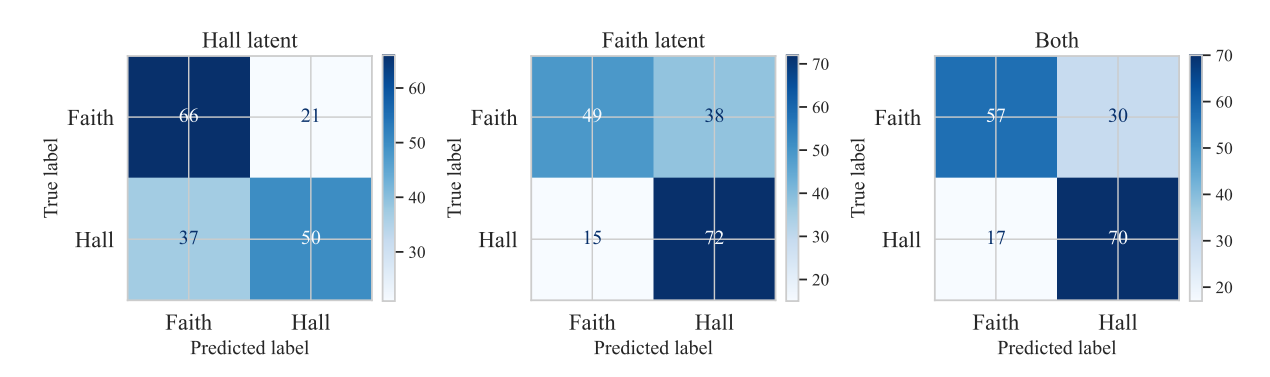


Figure 9: The confusion matrices for three main feature groups.

	$CHAIR_S\downarrow$	$\mid$ CHAIR $_I\downarrow\mid$	Avg.Len
LLaVA-NeXT	29.60	8.03	165.61
w/ SSL $\gamma = 0.2$	28.36	7.38	163.20
w/ SSL $\gamma = 0.4$	27.92	6.69	158.01
w/ SSL $\gamma = 0.6$	25.20	6.46	162.93
w/ SSL $\gamma = 0.8$	22.28	5.14	185.80
w/ SSL $\gamma = 1.0$	13.28	4.06	163.62
w/ SSL $\gamma = 1.5$	2.56	0.59	53.80

Table 5: Ablation study on the scaling factor of LLaVA-Next.

 $(\gamma=0.2)$  models, respectively. For LLaVA-Next, we observe that applying SSL at the middle layers more effectively mitigates hallucinations, consistent with the results shown in Figure 5. For LLaVA-1.5, we observe that applying SSL at either the layer1 or deeper layers consistently mitigates hallucination. This observation aligns closely with findings reported by Zhang et al. (2024b), He et al. (2024) and Chen et al. (2025), who also found that

layer1 or deeper layers interventions can significantly reduce hallucination in LLaVA-1.5. In contrast, for InstructBLIP, introducing SSL at shallow layers yields more substantial improvements, while deeper layer interventions contribute less noticeably to performance. We hypothesize that this is attributable to architectural and training differences in InstructBLIP, specifically, its shallow layers may already perform substantial cross-modal alignment early in the pipeline, making early-stage semantic guidance more impactful on overall generation quality. A deeper analysis of the layer-specific mechanisms in different multimodal architectures is left for future work.

# **D** Choice of Scaling Factor

Tables 5, 6, and 7 report the ablation results on the effect of the scaling factor  $\gamma$  in the SSL. For the LLaVA series of models, setting  $\gamma$  to 0.6 or 0.8 effectively reduces hallucinations, indicating

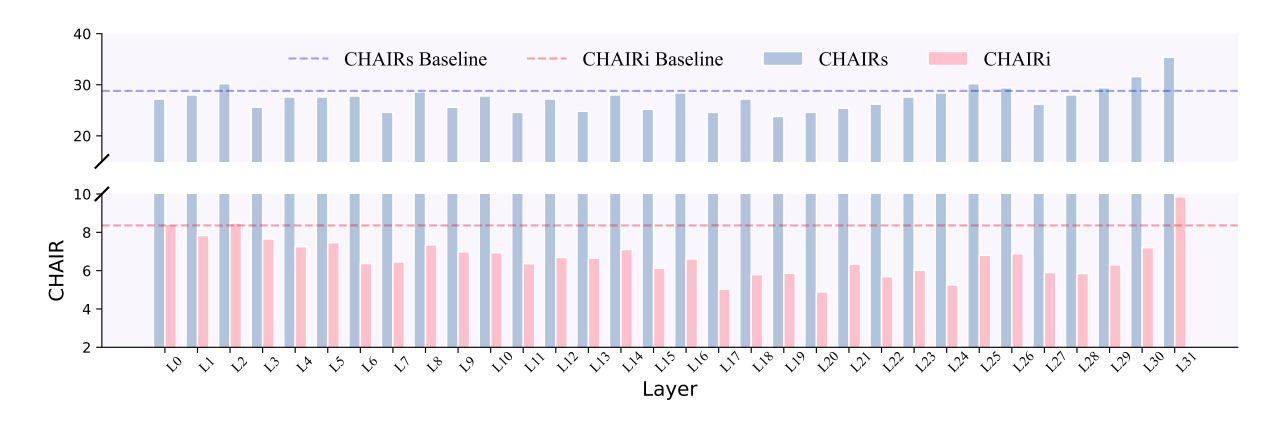


Figure 10: Ablation study on steering a specific layer of LLaVA-Next.

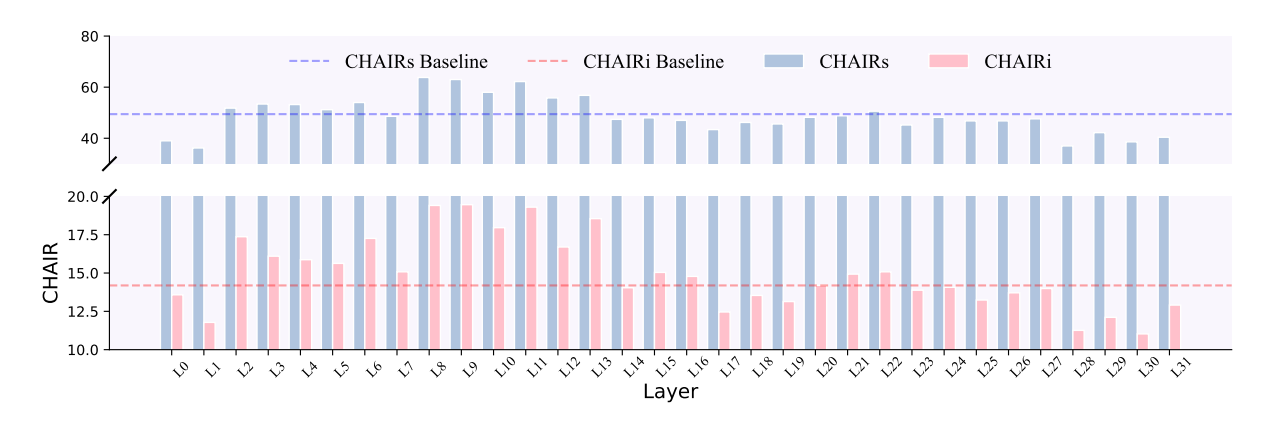


Figure 11: Ablation study on steering a specific layer of LLaVA-1.5.

Al	Algorithm 2: Reverse-SSL				
I	<b>Input:</b> Scaling factor $\gamma$ ; steering layer $l_s$ ;				
	semantic directions $d_{\text{hall}}$ , $d_{\text{faithful}}$ ;				
	residual stream at layer $l_s$ :				
	$[X_{l_s,s}, X_{l_s,t}, X_{l_s,v}, X_{l_s,o}^{< t}]$				
1 <b>if</b>	$1  ext{ if } L = l_s  ext{ then}$				
2	<b>for</b> token $x$ in residual stream <b>do</b>				
3	if $x \in X_{l_s,v}$ then				
4	$x \leftarrow x - \gamma \cdot \frac{\ x\ }{\ d_{\text{faithful}}\  + \epsilon} \cdot d_{\text{faithful}}$				
5	else if $x \in X_{l_s,o}^{<\iota}$ then				
6	$x \leftarrow x + \gamma \cdot \frac{\ x\ }{\ d_{\text{hall}}\  + \epsilon} \cdot d_{\text{hall}}$				
7	else				
	// System and prompt				
	// System and prompt tokens remain unchanged				

that moderate levels of semantic intervention are beneficial. However, when  $\gamma>1.0$ , the supervision becomes overly aggressive, disrupting the model's behavior and leading to abnormal hallucination metrics. In contrast, for InstructBLIP, the best performance is observed at  $\gamma=0.2$ , while

	$CHAIR_S\downarrow$	$\mathrm{CHAIR}_I\downarrow$	Avg.Len
LLaVA-1.5	49.44	14.19	82.97
w/ SSL $\gamma = 0.2$	48.16	14.10	83.45
w/ SSL $\gamma = 0.4$	47.16	14.04	83.24
w/ SSL $\gamma = 0.6$	45.96	13.36	83.63
w/ SSL $\gamma = 0.8$	41.08	12.02	82.30
w/ SSL $\gamma = 1.0$	33.80	10.18	86.02
w/ SSL $\gamma = 1.5$	17.16	7.66	275.16

Table 6: Ablation study on the scaling factor of LLaVA-1.5.

larger values similarly result in performance degradation. These findings highlight the importance of carefully calibrating the intensity of semantic guidance to balance model control and generation quality across different architectures.

# **E** Reverse-SSL Approach

To further validate the efficacy of the identified semantic directions, we extend the standard SSL by introducing Reverse Steering LVLMs via SAEs Latents (Reverse-SSL), an approach that deliberately induces the model to generate more hallucinations. Specifically, at each residual flow layer, we divide

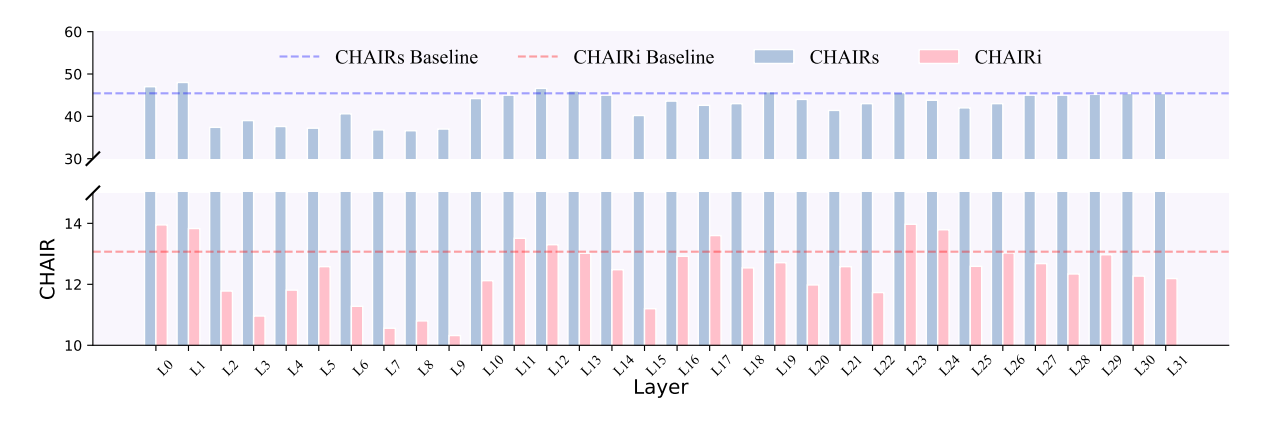


Figure 12: Ablation study on steering a specific layer of InstructBLIP.

	$CHAIR_S\downarrow$	$CHAIR_I\downarrow$	Avg.Len
InstructBLIP	45.44	13.07	92.11
w/ SSL $\gamma = 0.2$	38.52	11.45	102.62
w/ SSL $\gamma = 0.4$	10.16	7.90	64.04
w/ SSL $\gamma=0.6$	0.76	21.99	349.86

Table 7: Ablation study on the scaling factor of Instruct-BLIP.

the input sequence into four contiguous segments: system tokens, prompt tokens, visual tokens, and output tokens. During the visual-token stage, we inject a specific reverse-direction vector that deliberately shifts the visual features away from the true image semantics. At the onset of autoregressive language generation, we inject the specific reverse-direction to amplify the previously distorted visual signal, thereby biasing subsequent text outputs toward content that is either factually incorrect or substantially divergent from the original prompt. The complete algorithmic procedure for Reverse-SSL is presented in Algorithm 2.

# F More Qualitative Results

Figures 13, 14, and 15 present additional qualitative examples on the LLaVA-Next, LLaVA-1.5, and InstructBLIP models, respectively, to demonstrate the effectiveness of our proposed SSL approach in mitigating hallucinated objects. With the integration of SSL, the generated descriptions by LVLMs exhibit improved fidelity to the visual content while maintaining the richness and informativeness of the language output.

#### **G** Details on the GPT-40 Evaluation

To evaluate the performance of LVLMs on the LLaVA-Bench benchmark, we adopt GPT-40 as

the reference evaluator. Following the template provided in Table 8 of Gong et al. (2024), each evaluation instance includes the original image, the base output of the LVLM, and its SSL-enhanced counterpart. The evaluation focuses on both the accuracy and fineness of the generated responses. To mitigate potential biases caused by output order, we randomly swap the positions of the two outputs with a probability of 0.5 before each evaluation. Each sample is evaluated four times to compute an average score. Figures 16, 17, and 18 illustrate representative evaluation examples based on three model architectures: LLaVA-Next, LLaVA-1.5, and InstructBLIP, respectively.

# **H** License

The open-source data utilized in this work was employed exclusively for academic research, consistent with the original intended usage. All the used intellectual artifacts' license allows for academic usage.

#### **GPT-40 Prompt**

You are required to score the performance of two AI assistants in describing a given image. You should pay extra attention to the hallucination, which refers to the part of descriptions that are inconsistent with the image content, such as claiming the existence of something not present in the image or describing incorrectly in terms of the counts, positions, or colors of objects in the image. Please rate the responses of the assistants on a scale of 1 to 10, where a higher score indicates better performance, according to the following criteria:

- **1. Accuracy**: whether the response is accurate with respect to the image content. Responses with fewer hallucinations should be given higher scores.
- **2. Detailedness**: whether the response is rich in necessary details. Note that hallucinated descriptions should not count as necessary details.

Please output the scores for each criterion, containing only two values indicating the scores for Assistant 1 and 2, respectively. The two scores are separated by a space. Following the scores, please provide an explanation of your evaluation, avoiding any potential bias and ensuring that the order in which the responses were presented does not affect your judgment.

```
[Assistant 1]
{}
[End of Assistant 1]

[Assistant 2]
{}
[End of Assistant 2]

Output format:
Accuracy:
Reason:
Detailedness:
Reason:
```

Table 8: The prompt used for GPT-40 evaluation.



Please describe this image in detail.





Please describe this image in detail.



In the heart of a cozy room, a black and gray cat has found a comfortable spot on a wooden floor. The cat, with its fur as dark as night and patches LLaVA-Next as light as the moon, is facing away from us. To the left of the feline, a blue bicycle leans casually against a white wall. The bicycle, with its vibrant blue frame and black seat, adds a touch of color to the otherwise monochrome setting. The white wall behind it contrasts beautifully with the blue of the bicycle. The wooden floor beneath these objects adds warmth to the image, grounding the scene in a sense of homeliness.

In the image, a black and gray cat is the main subject, standing on a wooden floor. The cat is positioned in front of a bicycle wheel, which is leaning against a white wall. The bicycle wheel is black with a red brake, and it has a black tire. The cat is facing the wall, and its tail is raised, indicating that it might be curious or alert. The image also contains a text that reads Trackstar, which could be related to the bicycle or the cat. The overall scene suggests a domestic setting, possibly a home or a garage.



The image captures a serene and modern bathroom bathed in soft light. Dominating the scene is a white toilet, its lid closed, standing next to a shower enclosure. The shower, with its clear glass door, is adorned with a wooden shelf that holds a single red bottle. Next to the shower, there is a wooden cabinet with a mirror. The dark brown cabinet contrasts with the white countertop, which has a sink and a silver faucet. The floor has light beige tiles, and the walls are painted light gray. The layout is neat and makes the bathroom feel calm and modern.



The image captures a modern bathroom bathed in a soothing beige color scheme. The bathroom is wellequipped with a white toilet, a white sink, and a white shower. The shower is equipped with a wooden cabinet, providing storage space for toiletries. The sink is accompanied by a wooden warm glow on the beige tiles that cover the floor and walls. The overall layout of the bathroom suggests a well-organized and functional space.

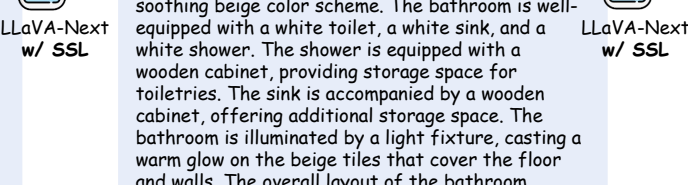


Figure 13: More examples of SSL in reducing hallucinated content in LLaVA-Next.



Please describe this image in detail.



Human

Please describe this image in detail.



The image features a large brown dog sitting on the floor in front of a flat-screen TV. The dog appears LLaVA-1.5 to be watching the TV, which is mounted on the wall above the dog. The TV is displaying a scene with a dog, likely capturing the dog's attention. In the room, there are two potted plants, one on the left side and the other on the right side. A remote control can be seen on the floor, close to the dog. Additionally, there is a book placed on the floor, slightly to the right of the dog.

The image features a large brown dog sitting on a carpeted floor in front of a flat screen TV. The dog LLaVA-1.5 appears to be watching something on the TV screen, w/ SSL likely a program or a movie. The TV is positioned on the left side of the room. Profiling the dog's position, there are two potted plants in the room, one on the right side and the other on the left side. The overall scene depicts a cozy and comfortable environment for the dog.

The image features a bathroom with a toilet situated on the left side of the room. A sink is located on the right side of the bathroom, and a mirror is mounted above it. The bathroom also has a large bowl-shaped sink, which is a unique and eyecatching design element. There are several toiletries placed around the bathroom, including a toilet paper roll, a toothbrush, and a cup. The toilet paper roll is positioned near the toilet, while the othbrush and cup are placed on the sink counter. The overall atmosphere of the bathroom is clean and well-organized.



The image depicts a bathroom with a large sink positioned under a mirror. The sink is made of a dark wood material, adding a touch of elegance to the space. The bathroom also features a toilet on the left side of the room. There are several towels in the bathroom, with one placed on the sink and two others positioned on the floor. Additionally, there is a roll of toilet paper on the sink, ensuring that the bathroom is well-stocked for its users.

Figure 14: More examples of SSL in reducing hallucinated content in LLaVA-1.5.



Figure 15: More examples of SSL in reducing hallucinated content in InstructBLIP.

The table is covered with a white cloth, providing a

clean and elegant setting for the pizza. <s>

heights, with one bench being slightly higher than

the others. The bushy shrubbery provides a natural

touch to the scene, adding a bit of greenery to the otherwise concrete-like environment. <s>

# [Input Image]



[Input Instruction]

Describe this photo in detail.

#### [Model Outputs]



The image is a digital artwork that pays homage to the famous painting \"Mona Lisa\" by Leonardo da Vinci. The central figure in the artwork is a dog, specifically a Chihuahua, dressed in a black dress with a white collar. The dog is wearing a brown headscarf and is seated against a backdrop of a landscape. The landscape features a river, mountains, and a castle. The dog's expression is neutral, and it is looking directly at the viewer. The artwork is a playful and creative take on the original painting, replacing the human subject with a dog.



LLaVA-Next w/ SSL

The image is a digital artwork that features a dog dressed in a style reminiscent of the Mona Lisa. The dog is depicted with a brown coat and a black face, with a large, expressive nose and eyes. It is wearing a brown headband and a dark brown shawl with a pattern that resembles the folds of the Mona Lisa's dress. The dog's arms are crossed, and it is looking directly at the viewer with a calm and serene expression. The background of the image is a landscape with a mountainous terrain, featuring a river winding through the mountains. The sky is filled with clouds, and the overall color palette is dominated by earth tones, with a focus on browns and grays. The painting style is reminiscent of the impressionist style, with loose brushstrokes and a focus on the interplay of light and shadow. The image is a playful and creative blend of the famous painting with the subject of a dog, combining elements of art history with a modern twist.

# Accuracy: 4.0 9.0

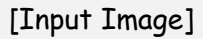


Reason: Assistant 1 inaccurately identifies the dog as a Chihuahua and mentions a black dress with a white collar, as well as a castle, none of which are present in the image. Assistant 2 accurately describes the dog in the style of the Mona Lisa, mentioning the correct attire and general description, with only minor inaccuracies like referring to the face as black instead of brown.

Detailedness: 5.0 9.0

Reason: Assistant 1 gives less accurate details and misses several aspects of the image, resulting in less informative content. Assistant 2 provides a detailed description of the image, including the style, attire, and background elements. It accurately conveys the artistic style and elements borrowed from the Mona Lisa.

Figure 16: The performance of SSL on reducing hallucinations on LLaVA-Next-8b.





[Input Instruction] What material appears to make up the creature?

# [Model Outputs]



The creature appears to be made of a combination of plastic and glass.



The creature appears to be made of a combination of materials, including a red or orange substance that resembles a horse or a camel, and a pair of eyeglasses. The overall appearance suggests that the substance is likely a combination of clay or a similar material, along with the eyeglasses, which add a creative and playful touch to the overall design.



Accuracy: 3.0 5.0

Reason: Assistant 1 accurately identifies the materials as plastic and glass, which may relate to the eyeglasses, but it doesn't address the fiery aspects or colors. Assistant 2 accurately describes the creature as having a red or orange appearance and mentions eyeglasses. However, the description of the material as clay is speculative and doesn't fully align with the molten, fiery appearance.

Detailedness: 2.0 6.0

Reason: Assistant 1 gives minimal description and lacks detail, primarily naming materials without describing the creature's form or distinctive features. Assistant 2 provides more details about the creature's appearance, color, and shape, mentioning both a horse or camel likeness and speculating on the material, despite some inaccuracies.

Figure 17: The performance of SSL on reducing hallucinations on LLaVA-1.5-7b.

# [Input Image]



[Input Instruction]

Describe this photo in detail.

#### [Model Outputs]



InstructBLIP

In the image, a man is standing on the back of a yellow car, ironing clothes on the roof. He is positioned on the right side of the car, with the laundry basket placed on the roof rack. The car is parked on a busy street, with several other vehicles and a truck in the background. The scene is set in a bustling city, with people walking around and cars passing by. The man's actions are likely to draw attention from the pedestrians, as he is ironing clothes on the roof of the car. <s>



The image shows a man in a yellow shirt standing on the back of a yellow SUV, ironing clothes on the roof of the vehicle. He is surrounded by various items, including a suitcase, a backpack, and a purse. The scene takes place on a busy city street, with multiple cars and a traffic light visible in the background. The man's presence on the roof of the SUV is a unique and creative way to iron clothes, making it a memorable and attention-grabbing image. <s>

Accuracy: 6.0 7.0



Reason: Both assistants correctly describe a man ironing on the back of a yellow vehicle. However, Assistant 1 inaccurately mentions the man standing on the roof and the presence of additional items such as a suitcase, a backpack, and a purse, which are not visible. Assistant 2 incorrectly mentions ironing on the roof, but doesn't add non-existent items, therefore has a slightly more accurate description..

Detailedness: 5.0 6.0

Reason: Assistant 1 provides some details, despite the inaccuracies, such as the mention of the city street and multiple cars, but includes incorrect additional items. Assistant 2 offers a more accurate context of the scene, noting the bustling city and people, though details about specific objects are still inaccurate. Both descriptions lack accuracy in detailedness, but Assistant 2 is slightly more coherent.

Figure 18: The performance of SSL on reducing hallucinations on InstructBLIP-7b.